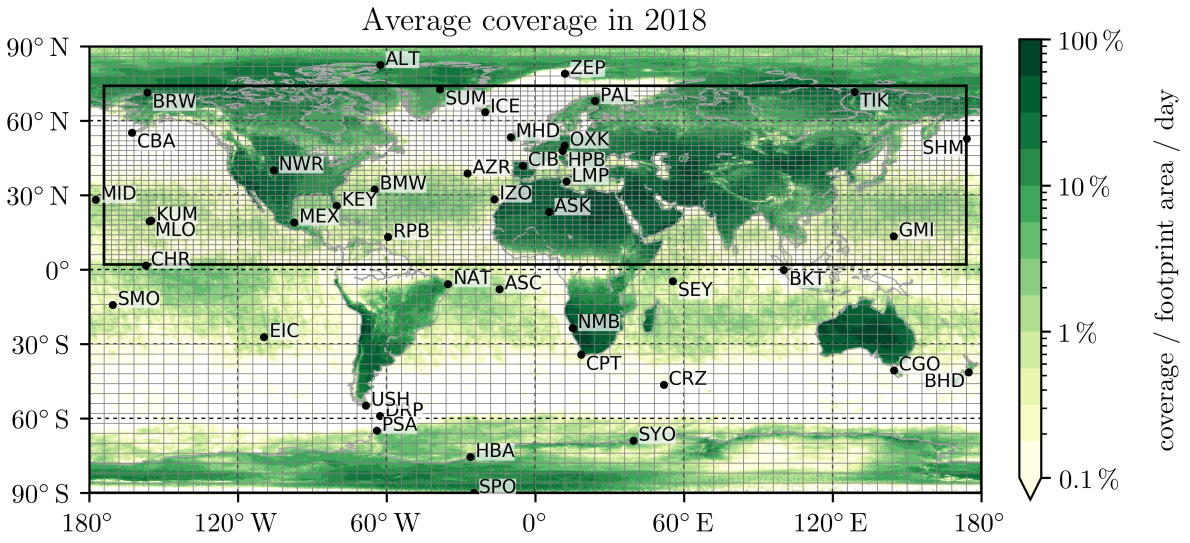

Figure S1. Daily average TROPOMI CO data coverage for 2018 after quality filtering, normed on the mean footprint area per observation ($\approx 84\,\mathrm{km}^2$). As in Figure 1 from the main manuscript, the nested zoom regions are shown as grids and the locations of the surface stations as dots.

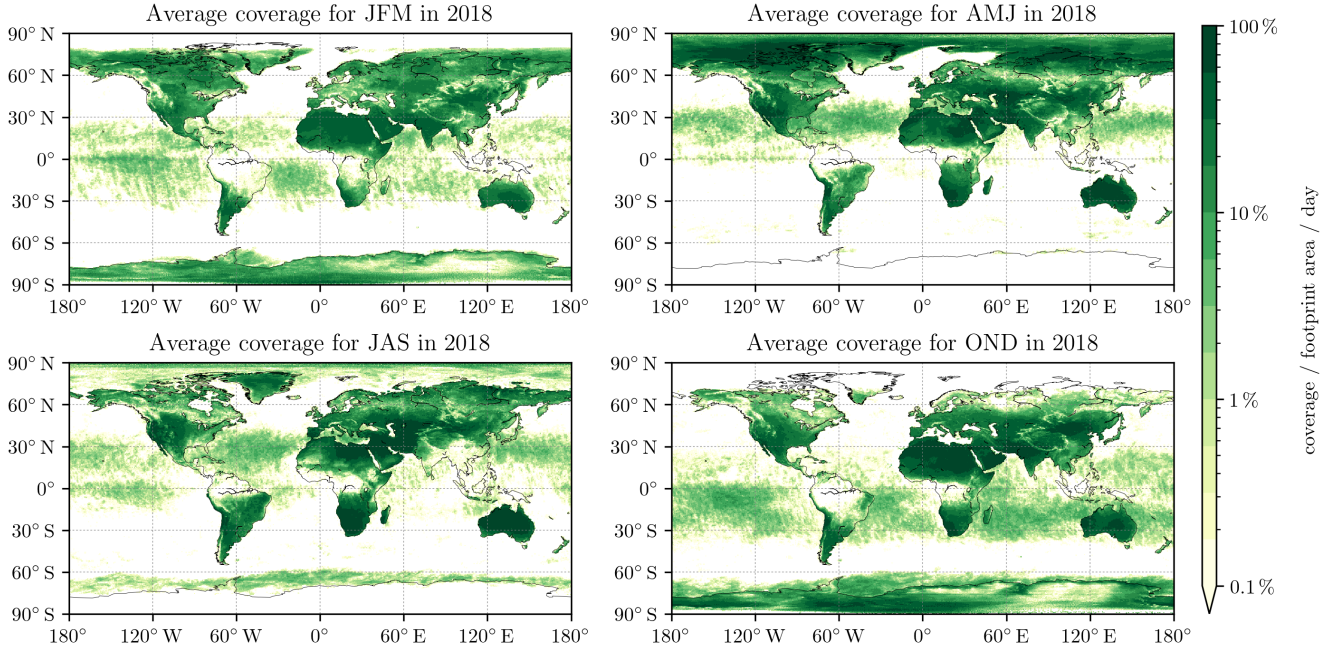

Figure S2. Same as S1, but split in 3 month periods to show seasonal variations.

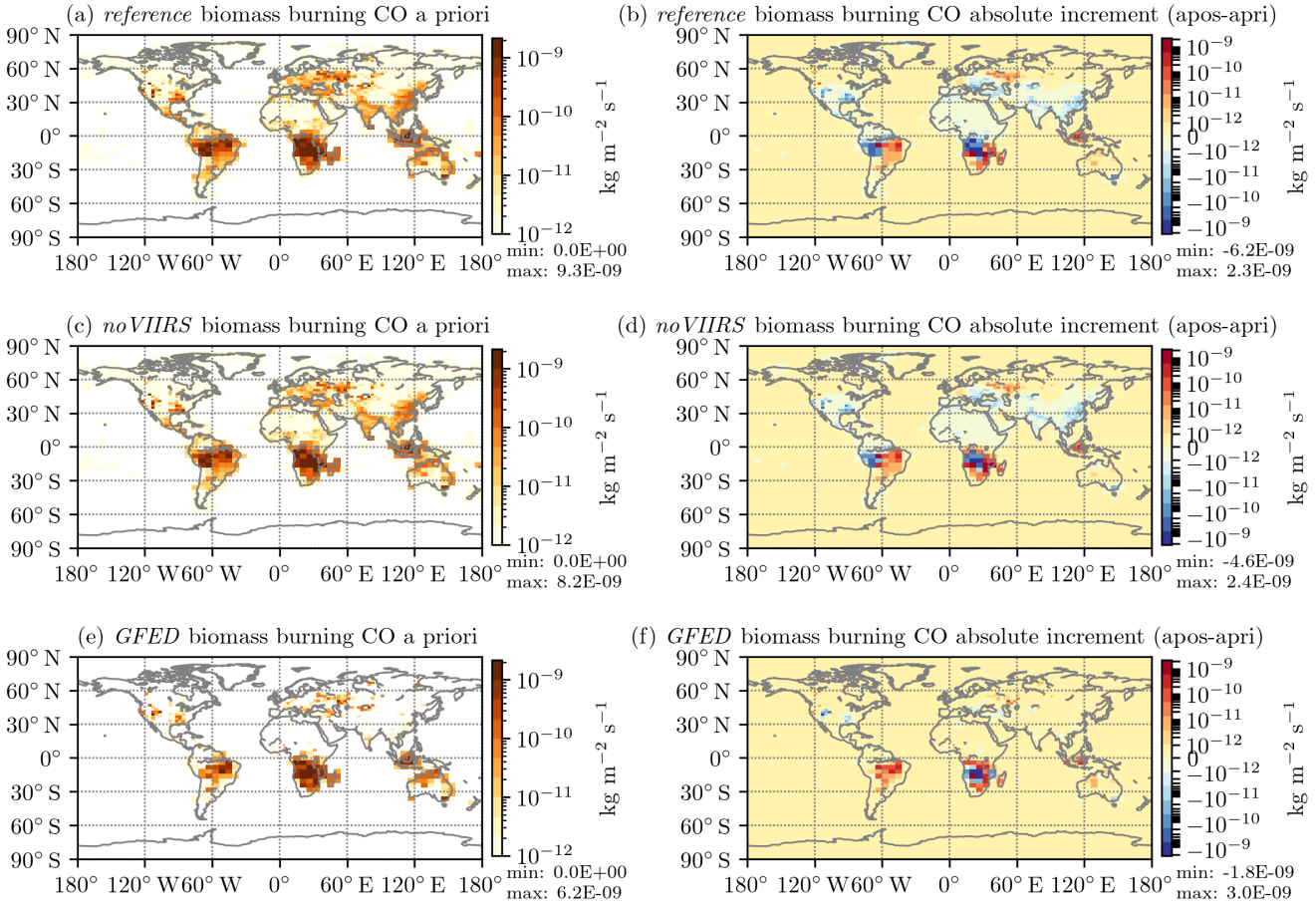

Figure S3. Global biomass burning CO emission for a single day, 15 September 2018, for the first set of inversions. The panels show the a priori emissions (left) and absolute emission increment (right) for the FINN2.4+VIIRS ((a) and (b)), FINN2.4 ((c) and (d)), and GFED ((e) and (f)) inventories.

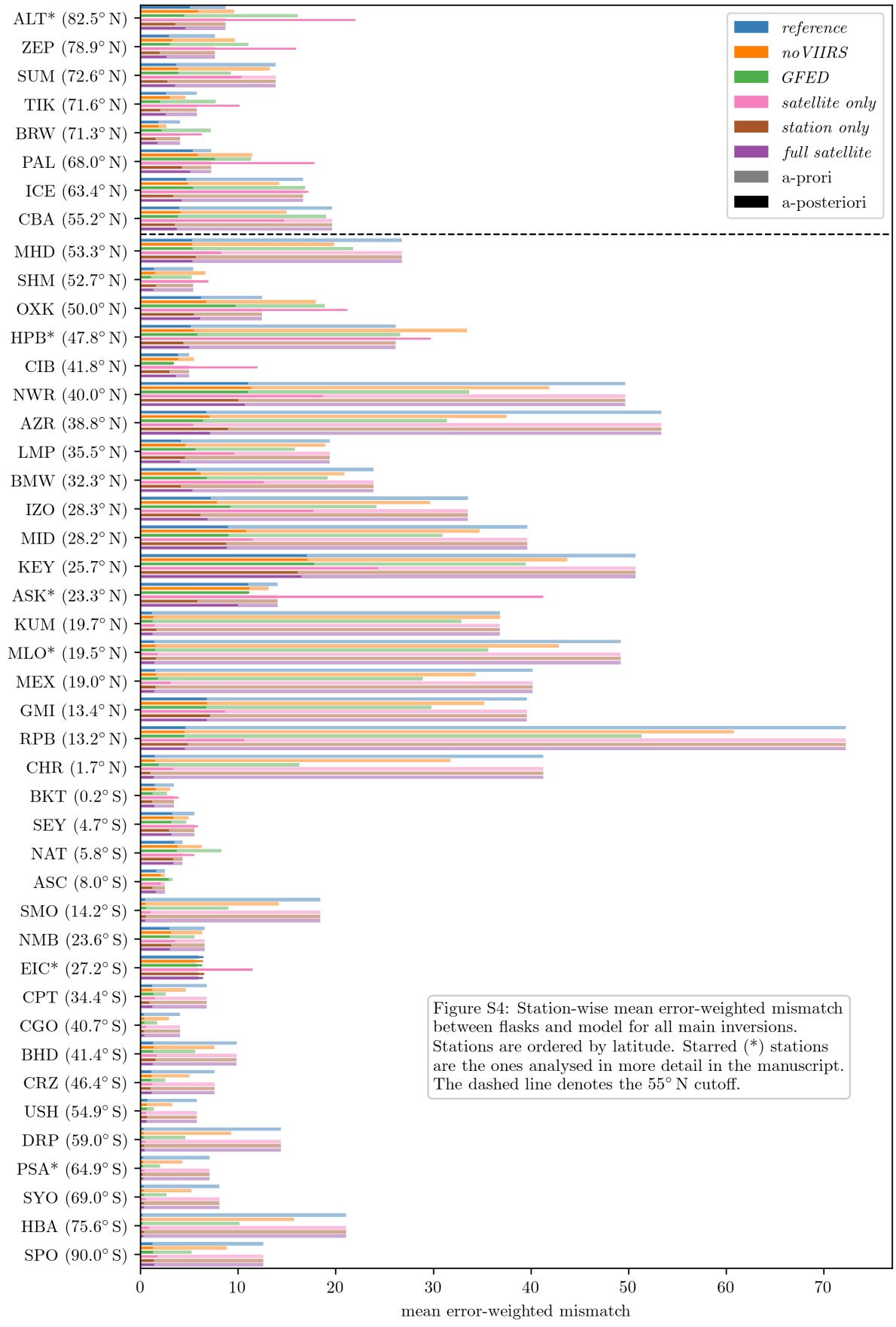

Figure S4: Station-wise mean error-weighted mismatch between flasks and model for all main inversions. Stations are ordered by latitude. Starred (*) stations are the ones analysed in more detail in the manuscript. The dashed line denotes the 55° N cutoff.

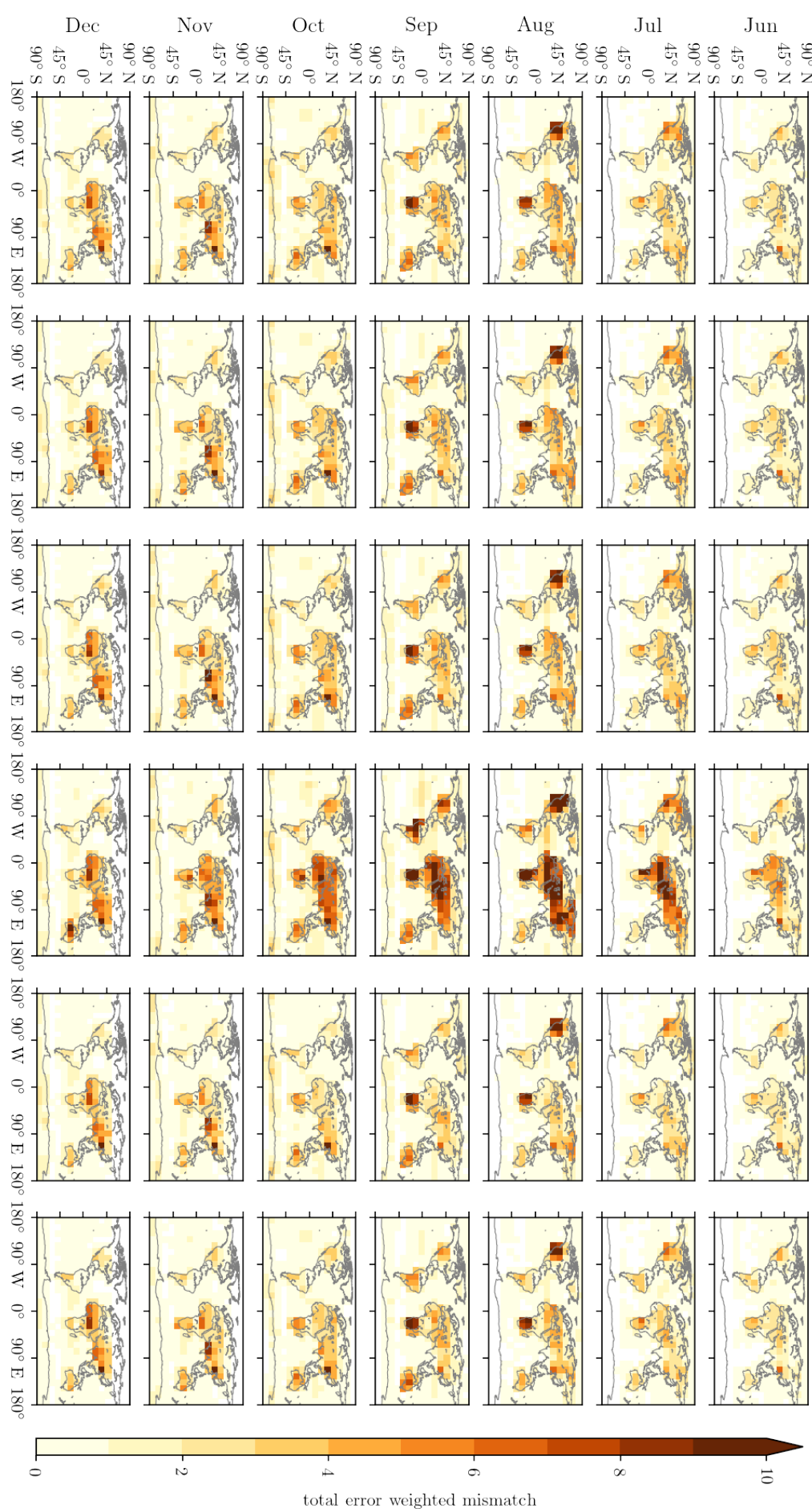

Figure S5. Total error-weighted mismatch between model and satellite observations aggregated in $12° \times 12°$ boxes and per month. This is equivalent to the contribution to the cost function from all observation in each box. The mismatches over the oceans are low because on the one hand there are fewer observations and on the other hand those observations represent the background mixing ratios, which are captured well by the model.

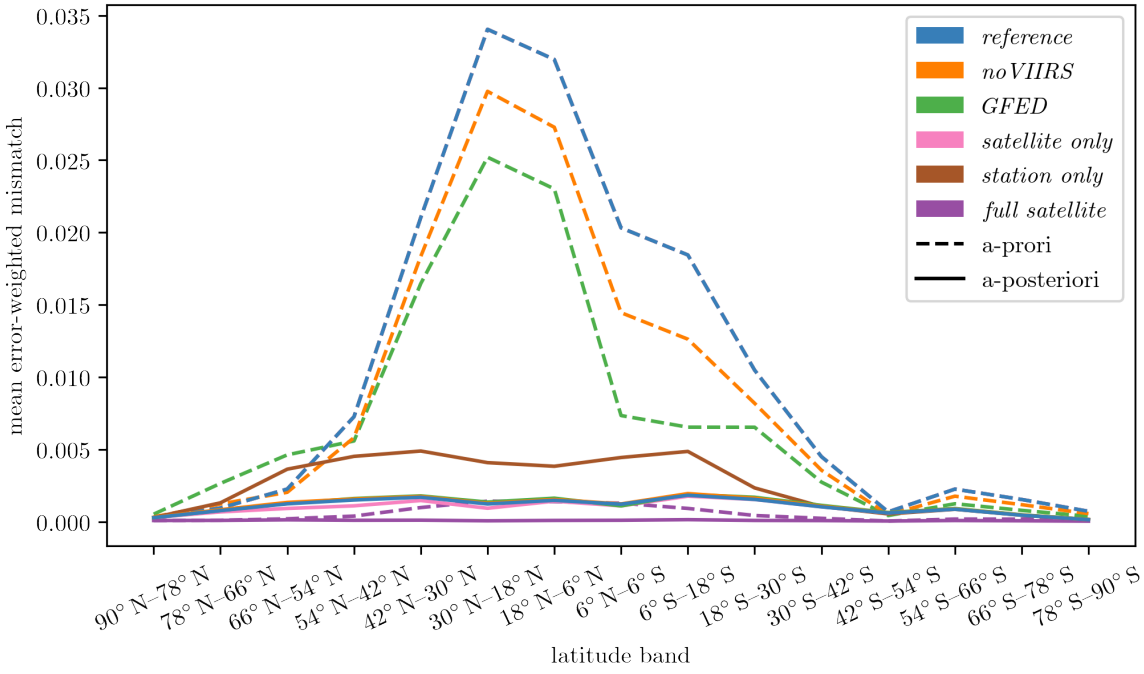

Figure S6. Mean a priori and a posteriori mismatch between the satellite and the model for all main inversions over the whole period aggregated in 12° latitudinal bands. A priori is larger, expect *station only* in high northern latitudes.

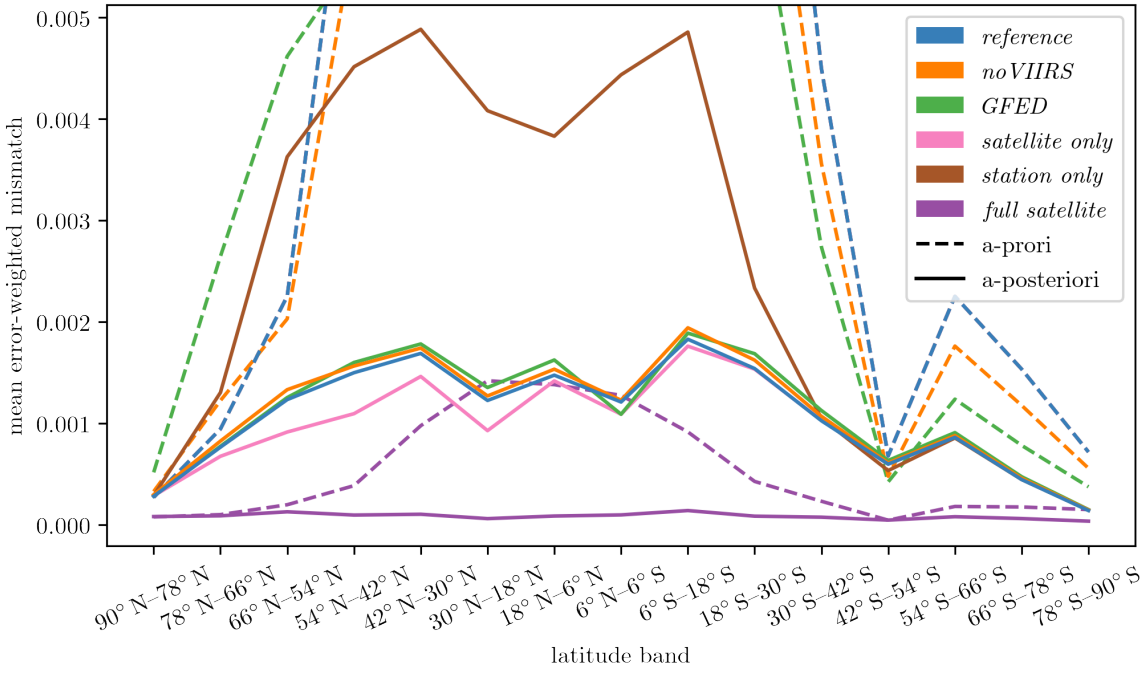

Figure S7. Same as above, but with the vertical axis scaled only by the a posteriori graphs, to make them more easily discernible. Clearly, all curves converge in the southern hemisphere.

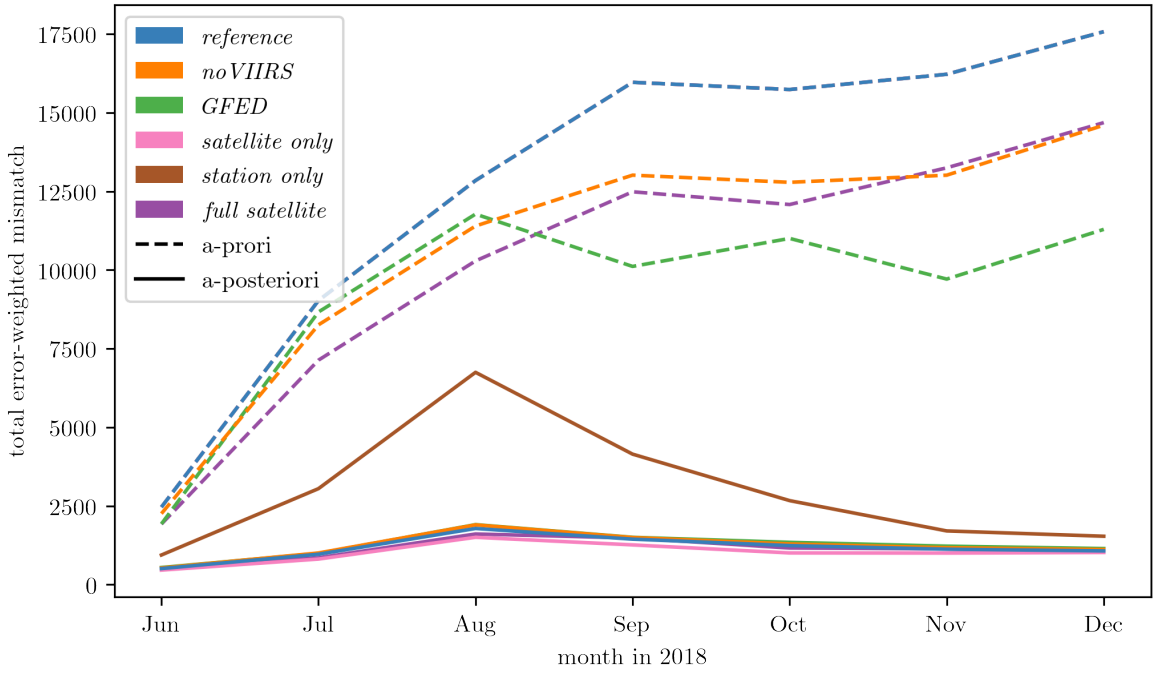

Figure S8. Total a priori and a posteriori mismatch between the satellite and the model for all main inversions. A priori mismatch only rises for the first two month of the inversion period and the reaches a plateau, pointing to the budget not being closed properly.

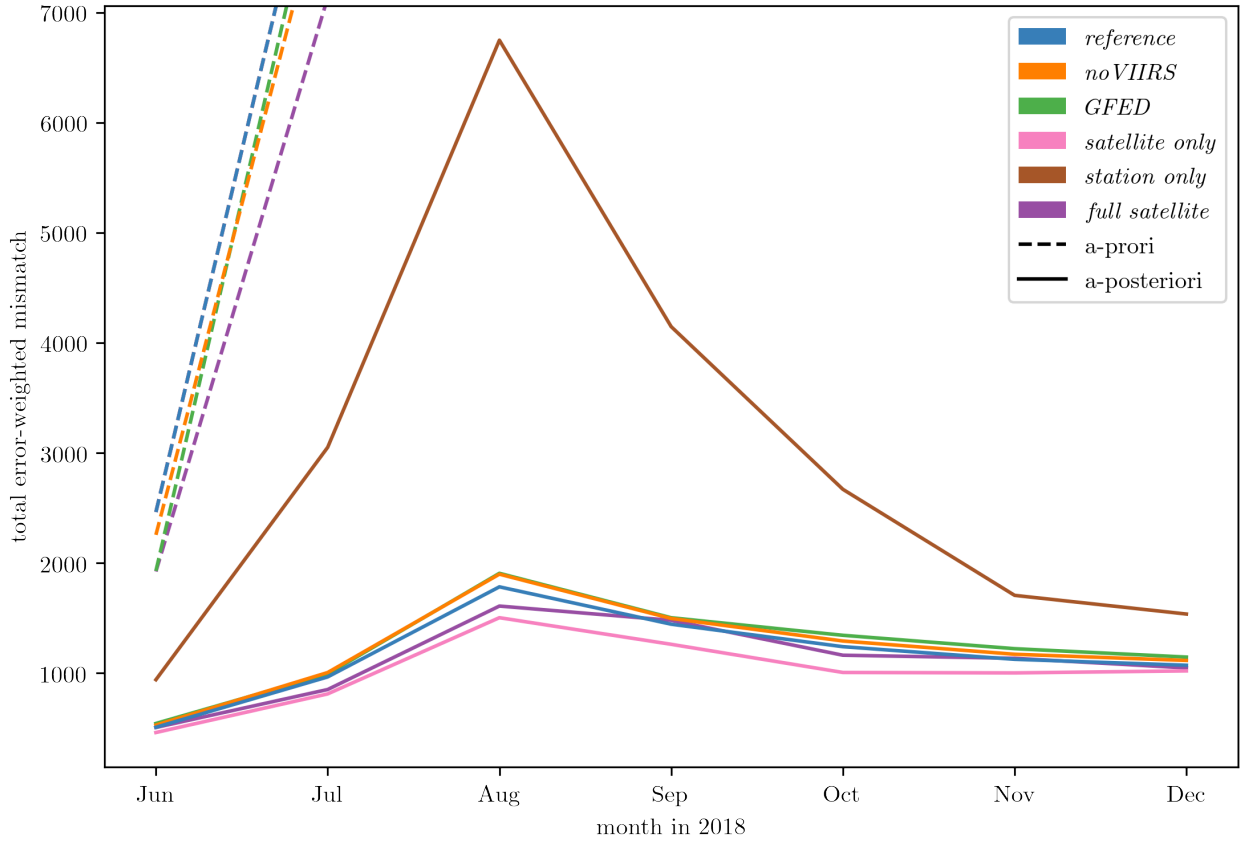

Figure S9. Same as above, but with the vertical axis scaled only by the a posteriori graphs, to make them more easily discernible. The increased mismatch during the main burning season (Jul-Aug-Sep) due to the models inability to properly capture local biomass burning events is clearly visible, especially in the *station only* inversion.

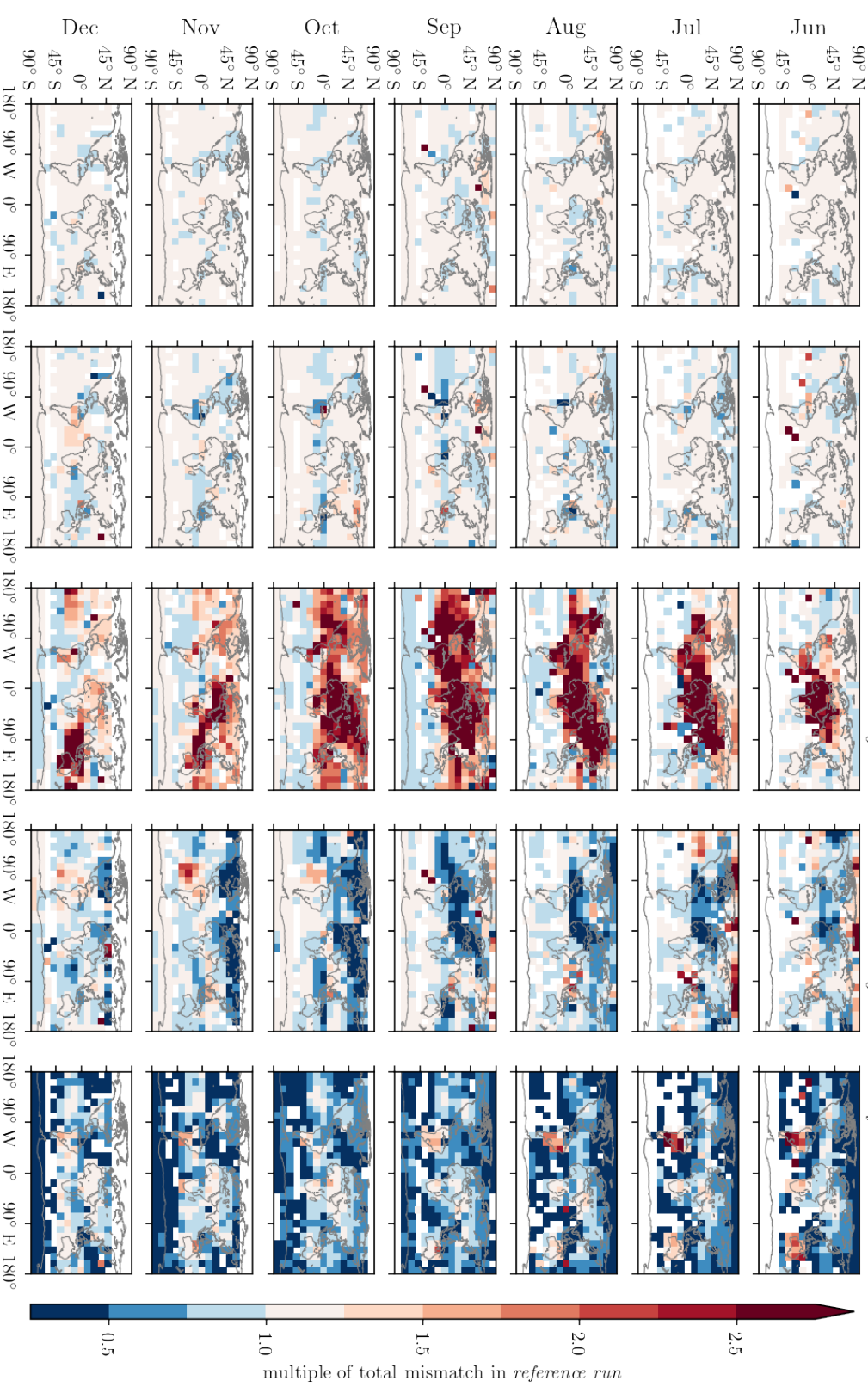

Figure S10. Total error-weighted mismatch between model and satellite observations aggregated in $12° \times 12°$ boxes and per month, divided by the corresponding mismatch of the *reference* inversion for that month. Red areas signify a worse fit than the *reference* inversion and vice versa for blue.

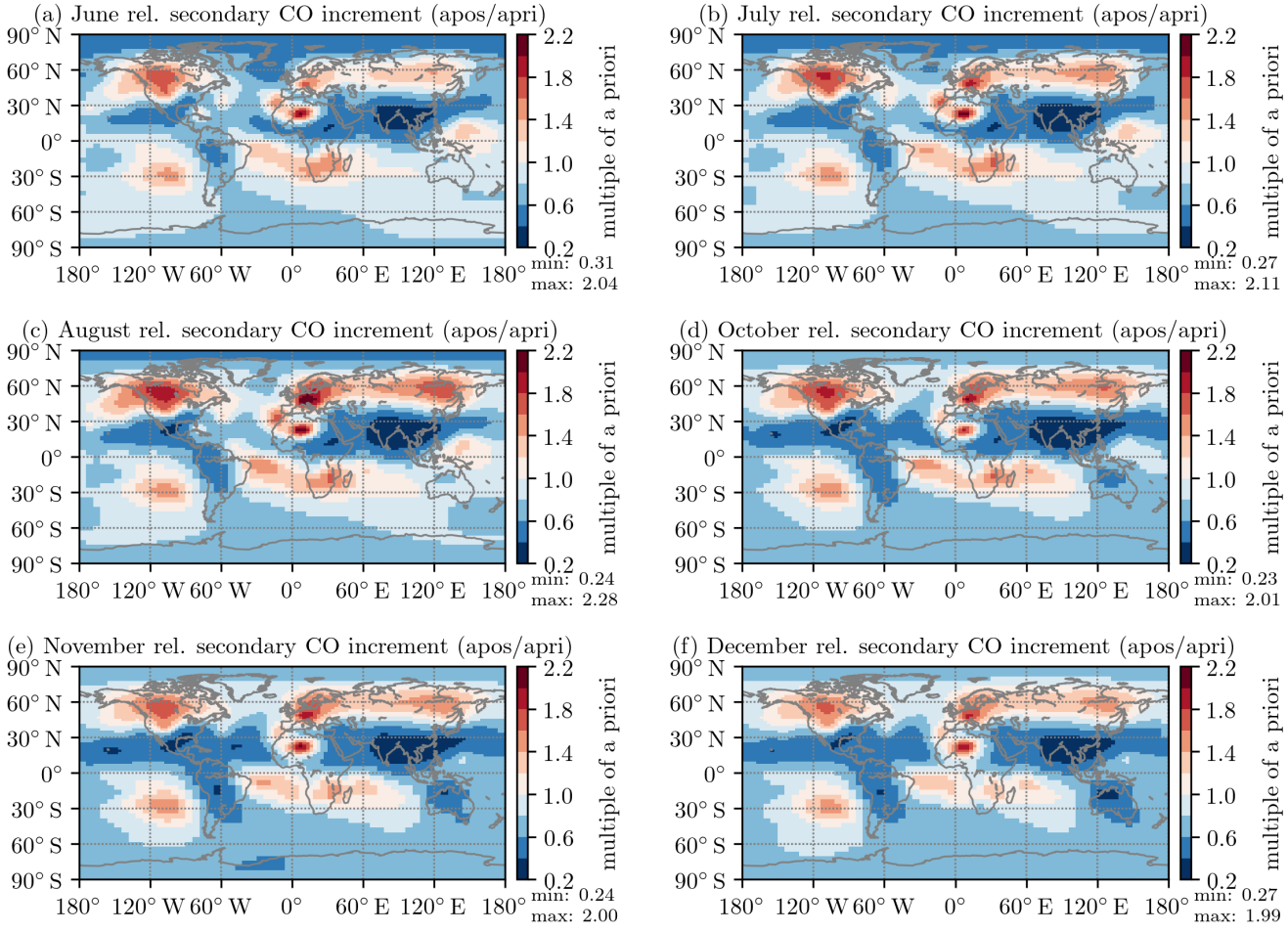

Figure S11. Global relative secondary CO emission increments resulting from the *reference* inversion for the remaining six months not shown in the main text. Overall, the global pattern of increments an decrements are preserved over time, only the amplitudes differ slightly. Most notably, the decrements in the remote northern hemisphere are more pronounced in the beginning of the inversion period, while those in the southern hemisphere are more pronounced towards the end of the period. The differences are shown in more detail in Fig. S12.

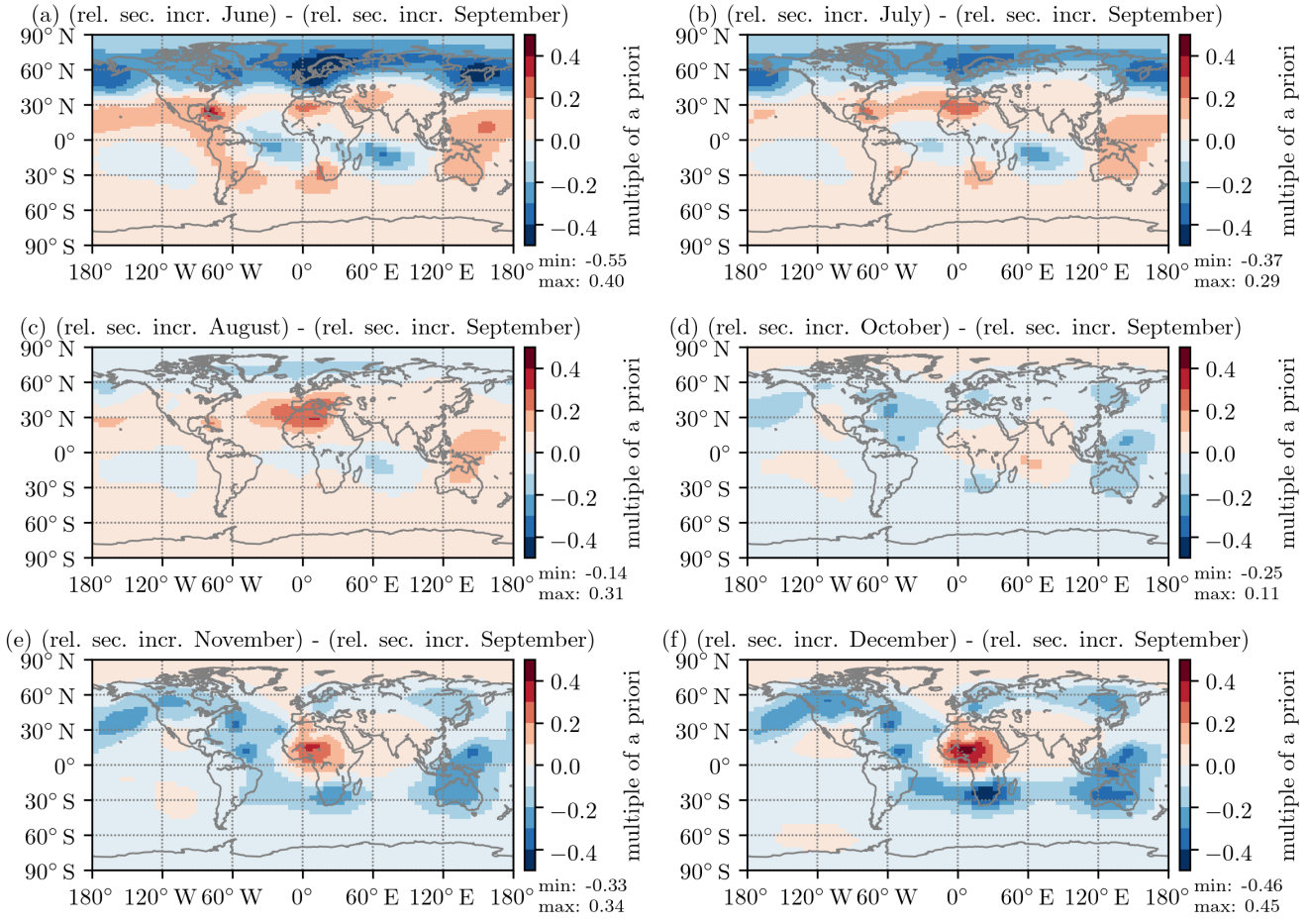

Figure S12. Differences in relative secondary CO emission increments resulting from the *reference* inversion between September (the month shown in Fig. 7 of the main text) and the remaining six months not shown in the main text (see also Fig. S11 above). Note the smaller range of the colorbar compared to Fig. S11. Interpretation of these plots is not trivial, since positive differences potentially imply a smaller/larger deviation from the prior, if the relative increments are smaller/larger than 1, but the so do negative differences, if the relative increments are larger/smaller than one. More details for the deviation from the prior are shown in Fig. S13.

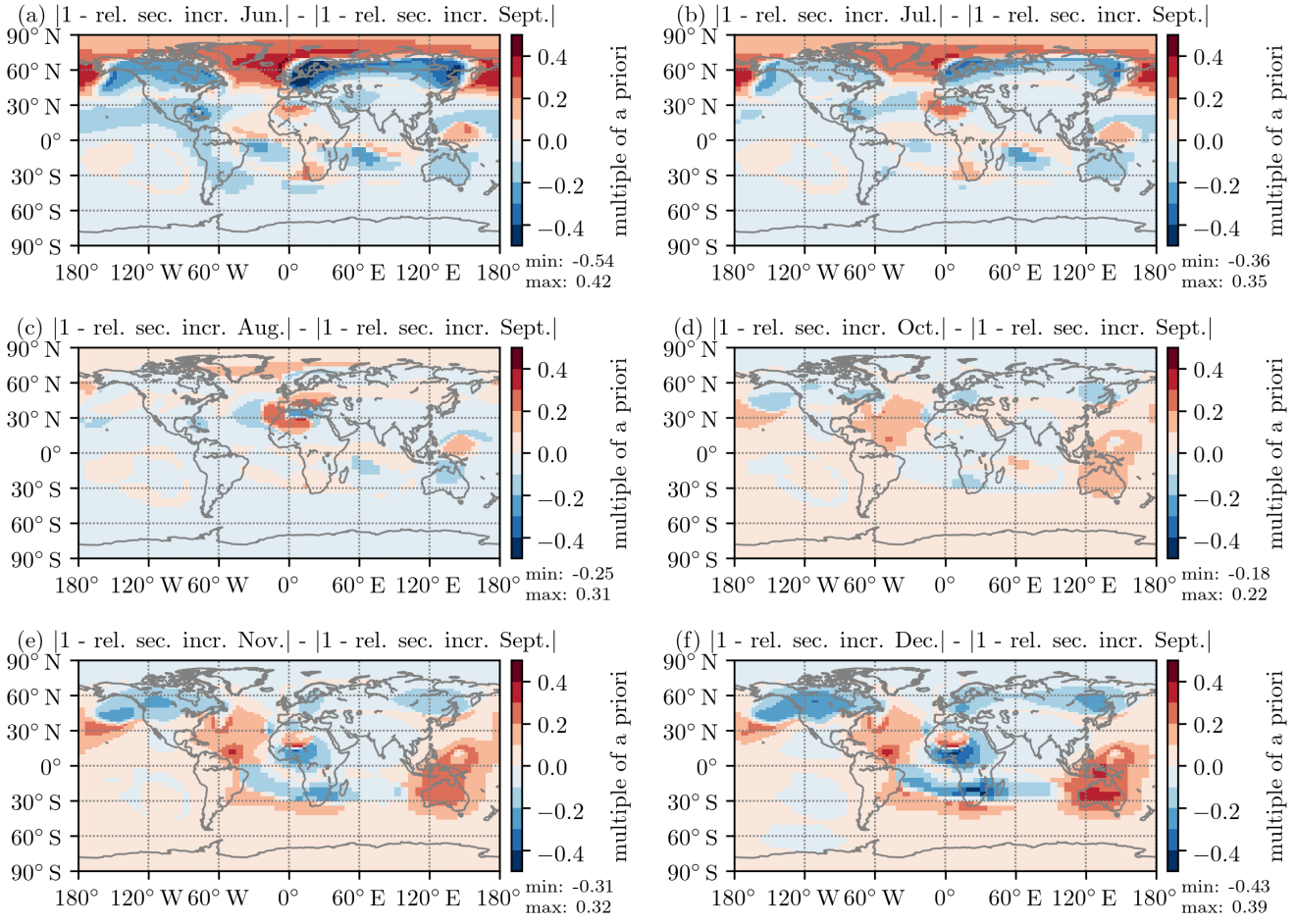

Figure S13. Differences in relative deviation from the prior for the secondary CO production for the *reference* inversion for September (the month shown in Fig. 7 of the main text) and the remaining six months not shown in the main text (see also Fig. S11 above). Red signifies areas were the relative increments deviate more from the prior than in September and vice versa for blue areas. Note that by taking the absolute value of 1 minus the relative increments, this does not contain information about whether the emission were increasing or decreasing anymore.

Table S1. Station-wise mean error-weighted mismatch between flasks and model.

station	*reference*		*station only*	*satellite only*	*full satellite*	*noVIIRS*		*GFED*	
	prior	poste	poste	poste	poste	prior	poste	prior	poste
ALT	8.71	5.08	3.55	22.03	4.63	9.62	5.93	16.10	4.47
ASC	2.50	1.63	1.21	2.07	1.59	2.52	2.11	3.27	2.88
ASK	14.05	11.02	5.81	41.27	9.98	13.11	11.17	11.04	11.15
AZR	53.37	6.76	8.98	5.47	7.11	37.55	7.09	31.39	6.42
BHD	9.86	1.28	1.54	1.69	1.26	7.59	1.36	5.63	1.31
BKT	3.44	1.47	1.17	3.90	1.43	3.05	1.60	2.71	1.25
BMW	23.88	5.71	4.15	12.64	5.33	20.90	6.15	19.18	6.78
BRW	4.04	1.85	1.56	6.31	1.73	2.69	1.86	7.20	2.16
CBA	19.66	3.98	3.51	14.69	3.74	14.98	4.12	19.02	3.86
CGO	4.05	0.38	0.35	0.57	0.42	2.91	0.39	1.72	0.40
CHR	41.26	1.46	0.98	3.35	1.37	31.79	1.50	16.29	1.87
CIB	4.97	3.83	2.97	12.01	3.63	5.49	3.89	3.34	3.45
CPT	6.80	1.20	0.91	1.46	1.19	4.63	1.18	2.60	1.34
CRZ	7.60	1.12	1.06	1.20	1.17	5.02	1.17	2.55	1.13
DRP	14.40	0.32	0.38	0.49	0.40	9.33	0.33	4.61	0.35
EIC	5.97	6.46	6.54	11.48	6.41	5.60	6.40	5.82	6.33
GMI	39.61	6.81	7.15	8.68	6.79	35.21	6.84	29.80	6.77
HBA	21.07	0.20	0.35	0.85	0.28	15.74	0.23	10.14	0.23
HPB	26.14	5.16	4.42	29.76	4.99	33.45	5.47	26.61	5.85
ICE	16.67	4.68	3.36	17.21	4.24	14.22	4.89	16.87	5.42
IZO	33.54	7.23	6.12	17.70	6.89	29.68	7.82	24.19	9.18
KEY	50.72	17.03	16.12	24.36	16.48	43.74	17.11	39.46	17.78
KUM	36.82	1.18	1.61	1.46	1.23	36.87	1.32	32.90	1.24
LMP	19.39	4.16	4.58	9.60	4.05	18.97	4.62	15.81	5.65
MEX	40.18	1.52	1.54	3.08	1.43	34.33	1.58	28.92	1.80
MHD	26.77	5.27	5.65	8.26	5.31	19.87	5.29	21.78	5.36
MID	39.63	8.99	8.75	11.51	8.86	34.76	10.84	30.94	9.01
MLO	49.19	1.41	1.59	1.76	1.43	42.89	1.54	35.67	1.49
NAT	4.30	3.48	3.35	5.52	3.41	6.28	3.81	8.32	3.72
NMB	6.60	2.99	3.13	3.56	3.00	6.33	3.13	5.52	3.01
NWR	49.70	11.04	10.01	18.72	10.71	41.89	11.33	33.67	10.99
OXK	12.46	6.22	5.43	21.22	6.14	17.98	6.75	18.90	9.72
PAL	7.26	5.37	4.23	17.85	5.12	11.44	5.88	11.33	7.62
PSA	7.09	0.28	0.26	0.39	0.27	4.32	0.28	2.02	0.28
RPB	72.27	4.60	4.88	10.67	4.56	60.80	4.54	51.36	4.50
SEY	5.52	3.27	2.92	5.90	3.19	4.95	3.39	4.69	3.20
SHM	5.40	1.36	1.58	6.96	1.32	6.68	1.52	5.25	1.06
SMO	18.42	0.51	0.52	0.98	0.49	14.19	0.54	9.03	0.59
SPO	12.57	1.27	1.38	1.70	1.42	8.85	1.30	5.26	1.29
SUM	13.85	3.63	2.78	10.36	3.57	13.26	3.84	9.29	3.89
SYO	8.09	0.34	0.37	0.52	0.38	5.23	0.36	2.66	0.36
TIK	5.80	2.66	2.01	10.14	2.61	4.62	3.03	7.71	1.99
USH	5.78	0.68	0.64	0.57	0.61	3.25	0.67	1.37	0.67
ZEP	7.61	2.95	1.98	15.94	2.69	9.67	3.27	11.07	3.01